# A Mobile Localization Algorithm based on Fuzzy Estimation for Serious NLOS Scenes

Yan Wang[1*], Yuxin Gong[1], Huikang Yang[1]

1. Department of Computer and Communication Engineering, Northeastern University, Qinhuangdao 066004, Hebei Province, China.
*Corresponding author: Yan Wang, E-mail: wangyan_jgxy@neuq.edu.cn, Telephone Number: +86-18894919682

***Abstract*—The indoor environment is intricate and the global positioning system (GPS) unable to satisfy the demand of indoor location accuracy. Therefore, the localization method based on wireless sensor network (WSN) has attach great importance and researched lately. The toughest issue to solve is the non-line of sight (NLOS) error caused by obstacles and other reasons. Hence, a location method based on hypothesis test and modified fuzzy probabilistic data association filter (HT-MFDAF) is proposed in this paper. Line-of-sight (LOS) and NLOS situations are regarded as an interactive Markov process. In the case of NLOS, we firstly identify and mitigate NLOS based on hypothesis testing theory. Then the ones which still have serious NOLS pollution is discarded by calculating similarity. Finally the fuzzy membership degree is calculated by MFDAF, reconstructing the correlation probability to get the position estimate. The eventual location result is acquired by the Interactive Multiple Model (IMM) which weighted LOS and NLOS estimated position. Simulation and experimental results demonstrate the effectiveness of the algorithm.**

***Index Terms*—indoor localization; non-line of sight; hypothesis test; fuzzy probabilistic data association filter.**

## I. INTRODUCTION

Wireless sensor network (WSN), as the hotspot of current international research, have been widely used in military[1], target tracking [2], monitoring [3], energy-efficient routing [4] and so on. Location based on WSN, which can make up for shortcomings of GPS indoor positioning accuracy, is one of the crucial elements for WSN. And it is mainly achieved by measuring the distance between the mobile node (MN) and the beacon node (BN). The main measurement methods include time of arrival [5], time difference of arrival [6], angle of arrival [7] and received signal strength [8] Moreover, LOS means that there is no barrier between BN and MN. Otherwise, it is NLOS. However, NLOS is more common in reality, especially in indoor environment, which is the main reason affecting the positioning accuracy.

On that basis, numerous algorithms and approaches have been researched. NLOS recognition is a research focus [9]-[16]. In [9]-[10], the identified NLOS measurements are discarded. A chi square test is proposed in [9] to identify NLOS situation. Then only measured values under LOS situation is used for positioning. [10] identifies and discards NLOS measurements by a threshold determined by NP theorem. This kind of approach availably removes impacts of NLOS measurements, but the location errors will sharply rise if the quantity of LOS BNs is not enough. To deal with this problem, creating virtual base stations (VBS) in uncharted region is presented in [11]. And VBS are generating by mirroring the NLOS BS on the transmitting wall, which are able to consider as LOS BS. Therefore, there will be sufficient BSs to ensure accurate positioning. Another approach is to use appropriately weighted LOS and NLOS measurements [12]-[14]. In [12], a GIMM-EKF method is proposed, where the Gaussian mixture model is used to identify LOS and NLOS. Moreover, feature matching also can reduce NLOS error, which is based on the pre-created databases, such as offline training [13]-[14]. But if the weight of NLOS is large, the positioning accuracy will be dramatically reduced. Due to the occlusion of obstacles, the NLOS measurements always have a positive deviation. Thus, it can be used as constraints or to mitigate NLOS errors to improve localization accuracy [15]-[16]. In [15], a cooperative localization algorithm is proposed. The geometric relationship of distance deviation is used to alleviate NLOS error, which also used as a constraint in semi definite programming. And the constrained Cramer Rao bound is derived, which is proved that it can effectively reduce NLOS errors. In [16], a through-the-wall (TTW) model is proposed, which focuses on reducing NLOS errors caused by walls. It describes the relationship between LOS and NLOS through the relative dielectric constant and thickness of the wall. Simulation reflects better positioning accuracy of the model.

On the other hand, [17]-[20] do not require NLOS identification for location under mixed LOS-NLOS conditions. Interacting multiple mode (lIMM) designs two parallel filters for LOS and NLOS models which are predicted at the same time. The final output values of the two models is obtained by weighted fusion of likelihood function and transition probability, which efficiently mitigates the NLOS effects. Therefore, numerous localization algorithms combined with IMM model have been proposed, such as kalman-based [17] and unscented kalman filter-based [18] IMM. Moreover, another extreme beneficial method is weighted least squares weighted least square (WSL) [19]-[20].In [19], a location method under unknown model is proposed, which derivates an equilibrium parameter and additional path loss. The unknown

parameters and positions are solved by robust weighted least square (RWLS) iteration. In [20], the variance of the estimated range is obtained by M estimation or MM estimation, which is used to calculate weights. Then the location is estimated by WSL and extrapolated single propagation UKF. It is worth noting that these methods use all the measured values, especially the IMM model, which requires a lot of calculation when there is a quantity of BSs.

Recently, fuzzy theory is widely used in target tracking and location. Fuzzy inference [21]-[22] and fuzzy clustering [24]-[26] are the two most commonly used techniques. [21] proposes a selective adaptive method for adjusting noise covariance using fuzzy logic, which use IMM to locate. Then the author extends the algorithm [22]. In this algorithm, EKF is added on the original basis. And the fuzzy-tuned EKF bank with NLOS bias is used for state estimation, which significantly improves the positioning accuracy. In [23], RSS is used to calculate the distance between MN and BN, which is nonlinear and obtained by interpolating several linear equations by fuzzy technology. Additionally, fuzzy clustering is mainly used for data association [24]-[26], using the similarity characteristics of fuzzy membership degree and correlation probability. Such as fuzzy c-means clustering [24] and maximum entropy fuzzy clustering [25]. In [26], the concept of rough set is introduced, which is combined with fuzzy set to calculate the incidence matrix. These methods greatly reduce the complexity of probabilistic data association (PDA), but unfortunately, the accuracy is not better than PDA.

In this paper, we propose a modified fuzzy PDA filter and make a NLOS recognition and mitigation of the initial distance measurements by hypothesis testing. Then the location estimation that still has NLOS errors are rejected by calculating the similarity. Finally, MFPDAF is used to calculate corresponding fuzzy memberships to get final estimated location under NLOS model. The contributions of our algorithm are as follows:

1) A NLOS recognition and mitigation method is proposed, which depends on the different distribution of measurement noise and NLOS noise and has a distinct mitigation performance on the measurement distance contaminated by NLOS.
2) The distance is processed in advance and then serious NLOS pollution points are discarded. Therefore, the algorithm has, especially in the serious NLOS scenes, superior performance, which is proved by simulations and experiments.
3) The algorithm can be easily expanded to multi-target tracking. And compared with traditional data association filter (DAF), MFDAF has lower computational cost and complexity.

The structure of the paper is organized as below. Signal model is introduced in Section II. Section III introduces the proposed algorithm in detail. In Section IV, we design the comparative simulation and experiment, and give the results. In Section V, we summarize the algorithm and describe the future work.

## II. Signal Model

### A. Signal Model

MN is assumed to move in a plane area with $N$ beacon nodes (BNs). The location of the BNs is known. And the transmission channels between the MN and the BN changes between LOS and NLOS conditions, which is denoted as a two-state Markov process and as shown in Fig. 1 .

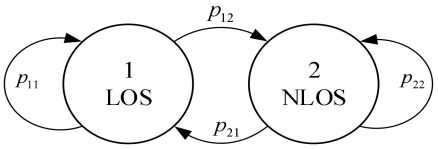


Fig. 1. Markov switching model.

The state vector of the MN is indicated as $X(s)=[x(s),y(s),\dot{x}(s),\dot{y}(s)]^T$ ,where $(x(s),y(s))$ and $(\dot{x}(s),\dot{y}(s))$ denotes the position and speed of the MN respectively and $s$ indicates a time step.

Then the state equation is modeled as

$$X(s)=FX(s-1)+Cv(s-1) \tag{1}$$

where,

$$F=\begin{bmatrix}1&0&T_S&0\\0&1&0&T_S\\0&0&1&0\\0&0&0&1\end{bmatrix} C=\begin{bmatrix}T_S^2/2&0\\0&T_S^2/2\\T_S&0\\0&T_S\end{bmatrix} \tag{2}$$

where, $T_s$ is the sampling period, $F$ denotes the state transition matrix of the MN. And $C$ is described the random acceleration caused by the process driving noise $v(s)$ that be assumed follow the Gaussian distribution $v(s)\sim N(0,\mathrm{Q}(s))$ .

In this paper, the distance between the MN and BN is obtained based on TOA at time step $s$, which can be defined as

$$r(s)=d(x(s))+n \tag{3}$$

where, $d(x(\mathrm{s}))$ is the real distance between BN and MN. And the noise n given by

$$n=\begin{cases}n_L & LOS\ \ condition\\ n_L+b_{NLOS} & NLOS\ \ condition\end{cases} \tag{4}$$

where, $n_L$ and $b_{NLOS}$ represent range and NLOS measurement noise respectively, which approximately follow the Gaussian distribution $n_L\sim N(0,\sigma_L^2)$ and $b_{NLOS}\sim N(\mu_n,\sigma_n^2)$ . Moreover the probability density function (PDF) of $b_{NLOS}$ can be derived as

$$f(b_{NLOS})=\frac{1}{\sqrt{2\pi}\sigma_n^2}\exp(-\frac{(b_{NLOS}-\mu_n)}{2\sigma_n^2}) \tag{5}$$

$d(x(s))$ can be expressed as

$$d_n(x(s))=\sqrt{(x(s)-x_{BS_n})^2+(y(s)-y_{BS_n})^2}\ \ n=1,2,...N \tag{6}$$

where, $(x_{BS_n},y_{BS_n})$ represents the coordinate of $n$ *-th* BN.

## III. PROPOSED METHOD

### A. The Main Procedures of the Algorithm

Fig. 2 illustrates the algorithm flow chart of this paper.

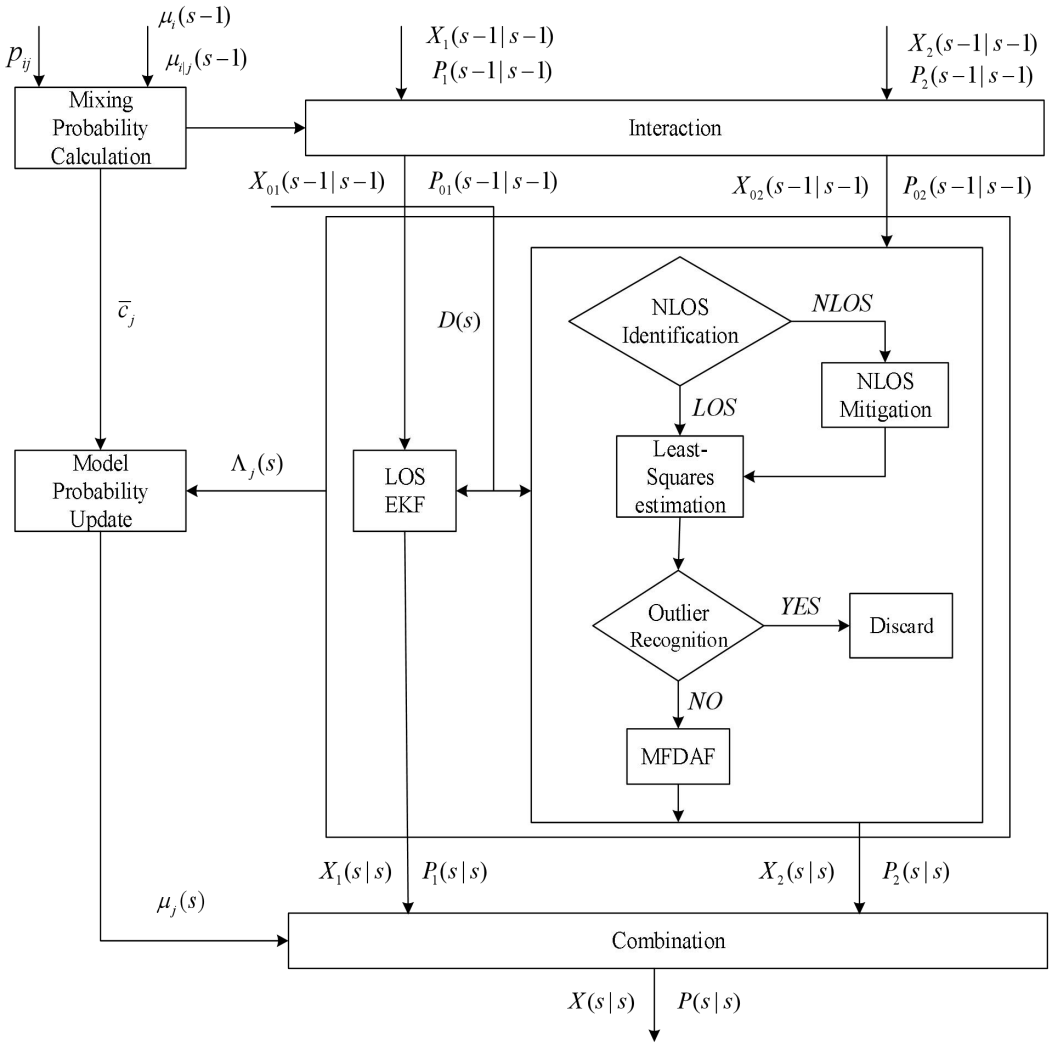


Fig. 2. Flow chart of proposed algorithm.

Firstly, we make a NLOS recognition and mitigation of the distance measurements by hypothesis testing. In this step, the mean $m_1$ and standard deviation (STD) $\sigma_1$ of the measured distance sequence before the current moment are calculated firstly (assuming that the sequence length is *M*). Then making current measurement minus $m_1$. The mean and variance of LOS and NLOS are different, so that we can compare the difference value with threshold that calculated by hypothesis testing to judge the current state. But once threshold ranges in the initial recognition is too small, which easily lead to wrong assumptions, hypothesis verification will be required. The mean $m_2$ and STD $\sigma_2$ of the measured distance sequence after the current moment (including the current moment) are calculated and then are compared with $m_1$ and $\sigma_1$, also making a comparison between thresholds and results to verify the hypothesis. When the current state is NLOS, the effect of the NLOS can be greatly eliminated by subtracting estimated bias from measurements. Then $C_N^3$ subgroups can be obtained when there are *N* BNs. Next the same number of estimated positions can be obtained by the least-squares (LS). Once more than one measurement of the subgroup is NLOS propagation, the position estimation should have deviation errors and outliers are generated. Since the more the coordinate points deviate, the smaller the corresponding similarity is. Therefore, outliers are found and discarded by calculating the similarity. Finally the fuzzy membership degree of the remaining position estimation is calculated by MFDAF, reconstructing the correlation probability to get the position estimate. The eventual location result is acquired by the IMM which weighted LOS and NLOS estimated position.

### B. Interaction and LOS update

1) *Interaction:* Firstly, the output of the LOS and NLOS model from the previous loop is interacted, which as the initial

state in the current loop. We assume that the state and covariance matrix interaction value of model $j$ separately express by $\hat{X}_{0j}(s-1|s-1)$ and $P_{0j}(s-1|s-1)$ .The interaction process is as follows

$$\hat{X}_{0j}(s-1|s-1)=\sum_i \hat{X}_i(s-1|s-1)\mu_{i|j}(s-1|s-1) \tag{7}$$

$$\tilde{X}_{ij}(s-1|s-1)=\hat{X}_i(s-1|s-1)-\hat{X}_{0j}(s-1|s-1) \tag{8}$$

$$\begin{aligned} P_{0j}(s-1|s-1)=\sum_i \mu_{i|j}(s-1|s-1)\{P_i(s-1|s-1) \\ +\tilde{X}_{ij}(s-1|s-1)\tilde{X}_{ij}^T(s-1|s-1) \end{aligned} \tag{9}$$

where, $\hat{X}_i(s-1|s-1)$ and $P_i(s-1|s-1)$ denote the state output value of filter $i$ at time $s$-$1$ and corresponding covariance estimation matrix. And $\mu_{i|j}(s-1|s-1)$ represents the mixed transition probability of model $i$ transferring to model $j$ at this time, which given by

$$\mu_{i|j}(s-1|s-1)=(1/\bar{c}_j)p_{ij}\mu_i(s-1) \tag{10}$$

where, $\bar{c}_j$ calculated by

$$\bar{c}_j=\sum_i p_{ij}\mu_i(s-1) \tag{11}$$

in particular, $i$ and $j$ belong to either 1 or 2, representing the LOS model and NLOS model respectively.

2) *Model matched:* The results of interaction between the two models, which obtained in the above process, are matched. Then the position and covariance of MN can be predicted through EKF, which can be calculated as

$$\hat{X}_j(s|s-1)=F\hat{X}_{0j}(s-1|s-1) \tag{12}$$

$$P_j(s|s-1)=FP_{0j}(s-1|s-1)F^T+CQ(s)C^T \tag{13}$$

*3) LOS Update:* Under the LOS model, the update process is achieved by EKF. Firstly, the innovation and innovation covariance matrix at time $s$ are calculated

$$V_1(s)=r(s)-d(\hat{X}_1(s|s-1)) \tag{14}$$

$$S_1(s)=H_1(s)\hat{P}_1(s|s-1)H_1^T(s)+R_1^*(s) \tag{15}$$

where, $R_1^*(s)$ is covariance matrix of the measurement error vector. And Jacobian matrix $H_1(s)$ in Eq. (15) is expressed as

$$H_1(s)=\left.\frac{\partial h(X(s))}{\partial(X(s))}\right|_{X(s)=\hat{X}(s|s-1)} \tag{16}$$

Then, the likelihood function under LOS model can be obtained

$$\Lambda_1(s)=N(V_1(s);0,S_1(s)) \tag{17}$$

And gain $K_1(s)$ is calculated by

$$K_1(s)=\hat{P}_1(s|s-1)H_1^T(s)S_1^{-1}(s|s-1) \tag{18}$$

Finally, the state variable estimation and error covariance matrix are modified based on Kalman gain matrix, which given by

$$\hat{X}_1(s|s)=\hat{X}_1(s|s-1)+K_1(s)V_1(s) \tag{19}$$

$$\hat{P}_1(s|s)=(I_4-K_1(s)H_1(s))\hat{P}_1(s|s-1) \tag{20}$$

### C. NLOS Identification and Mitigation

In the case of NLOS ($j=2$) we carry out NLOS recognition and mitigation that is shown in Fig. 3 for the initial measured distance. More detail will be described in the following section.

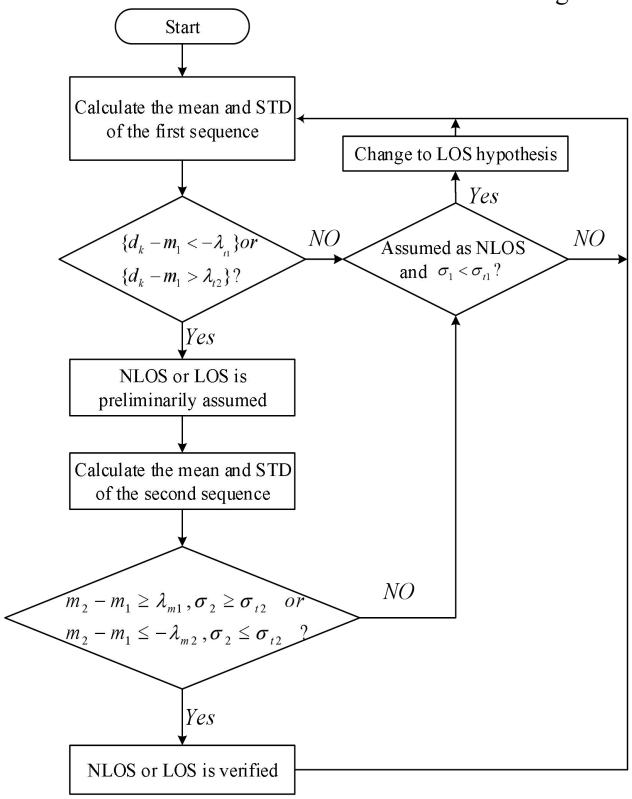


Fig. 3.Identification flowchart.

*1) Initial NLOS Identification:* Firstly, the mean $m_1$ and STD $\sigma_1$ of the measured distance sequence before the current moment are calculated, which can be expressed as

$$m_1=\frac{1}{M}\sum_{i=s-M}^{s-1} d_i \tag{21}$$

$$\sigma_1=\sqrt{\frac{1}{M}\sum_{i=s-M}^{s-1}(d_i-m_1)^2} \tag{22}$$

where, $M$ is the length of the sequence. Specifically, $M$ should be less than the samples per second of MN. For instance, if the sampling frequency is 5HZ, $M$ can be set to about 3. When the speed of MN is 1m/s, the change between the sequences is no more than 0.6m. It is guaranteed that there is an only minor change between sequences, especially compared to noise. Hence, the approach is uncomplicated and credible, having a minor effect on the STD calculation.

Suppose the distance at the current moment is denoted by $d_s$, which compared with $m_1$. On the one hand, if the difference is within a predetermined range, which is

$$-\lambda_{t1}<d_s-m_1<\lambda_{t2} \tag{23}$$

then the current measurement is assumed to be under NLOS state. But if

$$\sigma_1<\sigma_{t1} \tag{24}$$

the hypothesis is changed to LOS. $\lambda_{t1}$, $\lambda_{t1}$ and $\sigma_{t1}$ are threshold, that are discussed in section 3). Then the mean and STD in Eq. (21) and Eq. (22) are updated by $d_s$, which are used for the next

moment measurement and identification.

On the other hand, if Eq. (24) do not holds and

$$d_s - m_1 \geq \lambda_{t2} \tag{25}$$

the current propagation hypothesis is NLOS.

Moreover, while Eq. (23) is not satisfied, and

$$d_s - m_1 \leq -\lambda_{t1} \tag{26}$$

the LOS is supposed. Since there might be wrong decisions when $\lambda_{t1}$ and $\lambda_{t2}$ are small. Therefore, verifying the hypothesis is important, which can greatly enhance the correctness of decision-making.

*2) Hypothesis Verification:* To verify the decision that exceeds the threshold range, the mean and STD of the measured sequence after current moment are obtained by

$$m_2 = \frac{1}{M}\sum_{i=s}^{s+M-1} d_i \tag{27}$$

$$\sigma_2 = \sqrt{\frac{1}{M}\sum_{i=s}^{s+M-1}(d_i - m_2)^2} \tag{28}$$

The two sequences are shown in Fig. 4. In the following, we call the measurement of the first sequence $S_1$ and the second $S_2$.

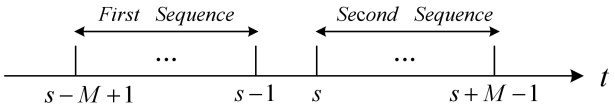


Fig. 4. Two measured distance sequences

When the Eq. (25) is true and

$$m_{2,1} = m_2 - m_1 \geq \lambda_{m1}, \quad \sigma_2 \geq \sigma_{t2} \tag{29}$$

then the current measurement is decided as NLOS. However, once a condition in Eq. (28) is not true, the assumption that time *s* is under NLOS propagation is rejected.

Similarly, if Eq. (26) holds and

$$m_{2,1} \leq -\lambda_{m2}, \quad \sigma_2 \leq \sigma_{t2} \tag{30}$$

where, $\lambda_{m1}$, $\lambda_{m2}$ and $\sigma_{t2}$ all are threshold. The current measurement will be decided as LOS. But the original LOS decision is also negated if one of the conditions in Eq. (30) is not true. Moreover, if both Eq. (29) and Eq. (30) are not satisfied, we return to check Eq. (24). And if Eq. (24) holds, the hypothesis is changed from NLOS to LOS.

3) *Threshold calculation:* In the above recognition and verification process, numerous thresholds are needed, which are calculated based on the hypothesis testing theory. In particular, the PDF of NLOS and LOS are different. So threshold can be determined accordingly when the probability of false alarm (PFA) is given. The distribution of noise is assumed to be a priori. In this case, the threshold is calculated in advance, so it doesn't take time. But the noise distribution in real scene may be unknown, which can be obtained by offline measurement and online estimation. This paper focuses on the known conditions.

Due to the occlusion of obstacles, the propagation time of NLOS will be longer, which is always positive errors. And it is usually assumed as a Gaussian, Rayleigh or exponential distribution when comparing the accuracy of localization algorithm. Thus, the measurement errors and NLOS errors are assumed as Gaussian distribution $N(0,\sigma_L^2)$ and $N(\mu_n,\sigma_n^2)$ respectively. Firstly, if $S_1$ is considered as LOS propagation. The mean and STD are zeros and $\sigma_L/\sqrt{M}$ accordingly. Hence, $f = d_s - m_1$ is still a Gaussian distribution which depends on whether the state of current moment is NLOS or LOS. If the current measurement is under LOS, the PDF of $f$ can be denoted as

$$p(f \mid los:los) = \mathrm{N}(0, \sigma_{\mathrm{LL}}^2) \tag{31}$$

where, $\sigma_{\mathrm{LL}} = \sigma_L\sqrt{1+1/M}$. On the other hand, when it is NLOS, the PDF is

$$p(f \mid los:nlos) = \mathrm{N}(\mu_n, \sigma_{\mathrm{LN}}^2) \tag{32}$$

where, $\sigma_{LN} = \sqrt{\sigma^2{}_L/M + \sigma_n^2}$.

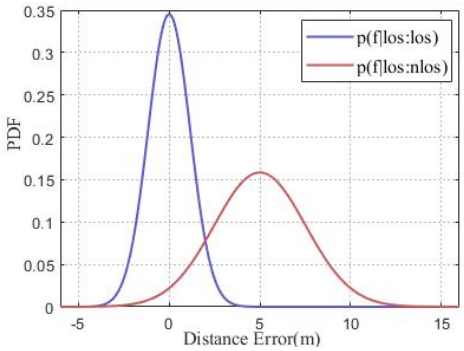


Fig. 5 An example of the two PDFs when NLOS is assumed.

Fig. 5 shows an example of the two PDFs in this case. We define the probability of detection (POD) as the probability of determining NLOS as NLOS, while PFA is the probability of determining LOS as NLOS. Explicitly, the two PDFs are overlap. Therefore, if a larger POD is required, the PFA will not be small enough, and vice versa. Therefore a trade-off should be made. And POD and PFA are respectively derived as

$$P_{FA} = \int_{\lambda_{t1}}^{\infty} \frac{1}{\sqrt{2\pi}\sigma_{LL}} \exp\left(-\frac{x^2}{2\sigma^2{}_{LL}}\right)dx = Q\left(\frac{\lambda_{t1}}{\sigma_{LL}}\right) \tag{33}$$

$$P_{\mathrm{D}} = \int_{\lambda_{t1}}^{\infty} \frac{1}{\sqrt{2\pi}\sigma_{LN}} \exp\left(-\frac{(x-\mu_n)^2}{2\sigma^2{}_{LN}}\right)dx = Q\left(\frac{\lambda_{t1}+\mu_n}{\sigma_{LN}}\right) \tag{34}$$

where, Q(*) is the standard Q-function. When a PFA or POD value is given, the threshold is calculated.

On the other hand, when the propagation state of $S_1$ is assumed to be NLOS, its mean and STD are respectively $\mu_n$ and $\sigma_n/\sqrt{M}$. Accordingly, when the current state is LOS or NLOS, the corresponding PDF is shown in Eq. (35) and Eq. (36)

$$p(f \mid nlos:los) = \mathrm{N}(-\mu_n, \sigma_{NL}^2) \tag{35}$$

$$p(f \mid nlos:nlos) = \mathrm{N}(0, \sigma_{NN}^2) \tag{36}$$

where, $\sigma_{NL} = \sqrt{\sigma^2{}_n/M + \sigma_L^2}$ and $\sigma_{NL} = \sigma_n\sqrt{1+1/M}$. Similarly, Fig. 6 describes the two PDFS

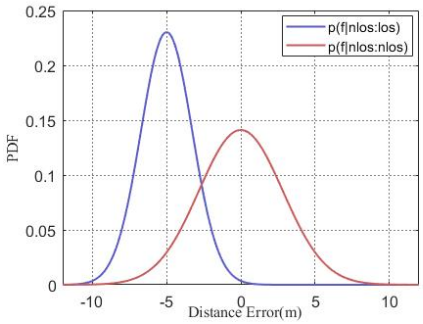


$$p(f \mid nlos:nlos) = \mathrm{N}(0, \sigma_{NN}^2)$$

Fig. 6 An example of two PDFs when LOS is assumed.

Then the POD and PFA can be derived as

$$P_{FA} = \int_{\lambda_{t2}}^{\infty} \frac{1}{\sqrt{2\pi}\sigma_{NL}} \exp(-\frac{(x+\mu_n)^2}{2\sigma^2_{NL}})dx = Q(\frac{\lambda_{t2}-\mu_n}{\sigma_{NL}}) \tag{37}$$

$$P_{\mathrm{D}} = \int_{\lambda_{t2}}^{\infty} \frac{1}{\sqrt{2\pi}\sigma_{NN}} \exp(-\frac{x^2}{2\sigma^2_{NN}})dx = Q(\frac{\lambda_{t2}}{\sigma_{NN}}) \tag{38}$$

It is worth mentioning that the bias mean is subtracted when the current measured distance is verified as NLOS. Hence, PFA should be kept in a smaller range, which is essential.

However, as we mentioned above, the initial decision may be wrong when the value of $\lambda_{t1}$ and $\lambda_{t2}$ are small. And the ideal PFA and POD values cannot be obtained simultaneously. For example, when required values are determined, we set the PFA at 95%, but the POD of this time is decreased to 66%. Therefore, it is indispensable to verify the hypothesis for resolving such a contradiction.

In the analysis for hypothesis verification, the threshold is calculated based on the mean difference $m_{2,1}$ between $S_1$ and $S_2$. Firstly, the case that $S_1$ is the LOS propagation state is analyzed. When $S_2$ is also in LOS propagation state, the PDF of $m_{2,1}$ is expressed as

$$p(m_{2,1} \mid los:los) = \mathrm{N}(0, \tilde{\sigma}^2_{\mathrm{LL}}) \tag{39}$$

where, $\tilde{\sigma}_{LL} = \sigma_L\sqrt{2/M}$ .

Then $S_2$ is under NLOS propagation, $m_{2,1}$ has a PDF given by

$$p(m_{2,1} \mid los:nlos) = \mathrm{N}(\mu_n, \tilde{\sigma}^2_{\mathrm{LN}}) \tag{40}$$

where, $\tilde{\sigma}_{LN} = \sqrt{(\sigma^2{}_n + \sigma^2{}_L)/M}$ . Fig. 7 shows the two PDFs in this case.

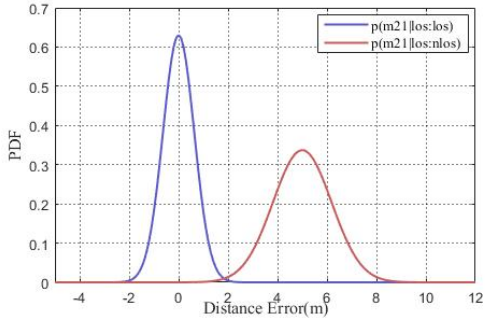


Fig. 7 An example of two PDFs for LOS hypothesis verification.

It is easy to observe that the two PDFs hardly overlap, even when the $M$ is small. The STD of $m_{2,1}$ is significantly reduced because of the averaging operation. Therefore, by selecting the appropriate threshold, we can almost always get the right hypothesis. PFA and POD correspond as follows

$$P_{FA} = \int_{\lambda_{m1}}^{\infty} \frac{1}{\sqrt{2\pi}\tilde{\sigma}_{LL}} \exp(-\frac{x^2}{2\tilde{\sigma}^2_{LL}})dx = Q(\frac{\lambda_{m1}}{\tilde{\sigma}_{LL}}) \tag{41}$$

$$P_{\mathrm{D}} = \int_{\lambda_{m1}}^{\infty} \frac{1}{\sqrt{2\pi}\tilde{\sigma}_{LN}} \exp(-\frac{(x-\mu_n)^2}{2\tilde{\sigma}^2_{LN}})dx = Q(\frac{\lambda_{t1}+\mu_n}{\tilde{\sigma}_{LN}}) \tag{42}$$

On the other hand, if the assumption of $S_1$ is in the NLOS propagation state, also the PDFs can be expressed as Eq. (43) or Eq. (44) respectively with $S_2$ in the LOS or NLOS.

$$p(m_{2,1} \mid nlos:los) = \mathrm{N}(-\mu_n, \tilde{\sigma}^2_{\mathrm{NL}}) \tag{43}$$

$$p(m_{2,1} \mid nlos:nlos) = \mathrm{N}(0, \tilde{\sigma}^2_{NN}) \tag{44}$$

where, $\tilde{\sigma}_{NL} = \sqrt{(\sigma^2{}_n + \sigma^2{}_L)/M}$ and $\tilde{\sigma}_{NN} = \sigma_n\sqrt{2/M}$ The two PDFs is shown in Fig. 8.

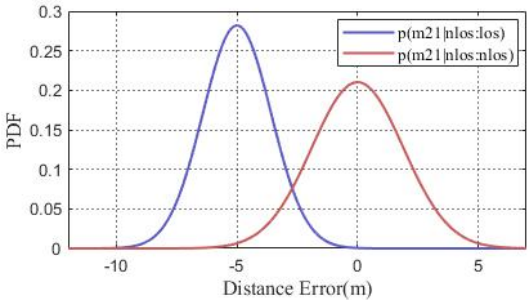


Fig. 8 An example of two PDFs for NLOS hypothesis verification.

It can be seen that the overlap of the two density functions is small, so as long as the appropriate threshold is selected, the decision in the first stage can be verified correctly. And the PFA and POD at this time are

$$P_{FA} = \int_{\lambda_{m2}}^{\infty} \frac{1}{\sqrt{2\pi}\tilde{\sigma}_{NL}} \exp(-\frac{(x+\mu_n)^2}{2\tilde{\sigma}^2_{NL}})dx = Q(\frac{\lambda_{t2}-\mu_n}{\tilde{\sigma}_{NL}}) \tag{45}$$

$$P_{\mathrm{D}} = \int_{\lambda_{m2}}^{\infty} \frac{1}{\sqrt{2\pi}\tilde{\sigma}_{NN}} \exp(-\frac{x^2}{2\tilde{\sigma}^2_{NN}})dx = Q(\frac{\lambda_{t2}}{\tilde{\sigma}_{NN}}) \tag{46}$$

As mentioned above, all thresholds are calculated by the $Q$ function which guided by the value of PFA and POD.

### *D. MFDAF*

*1) Outlier Detection:* At least 3 measured distances are needed when the location of MN is calculated by LS. Therefore, $R = C_N^3$ location estimates are obtained with $N$ BN at most, which denoted as $(\hat{x}_i(s), \hat{y}_i(s)), i = 1, 2, ..., R$

Although the measured distance has been processed above, the effect is not perfect. Consequently, there may be estimated coordinates with deviation errors, which can be called outlier that is shown in Fig. 9 .

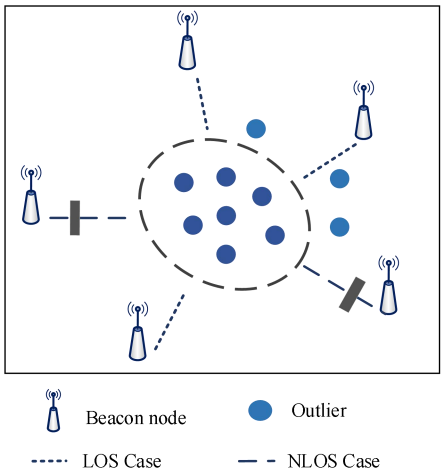

Fig. 9. Outliers generated by NLOS.

Firstly, the similarity $S_{ij}$ between two coordinate points is calculated as

$$S_{ij} = e^{-\alpha D_{ij}} \tag{47}$$

where, $D_{ij}$ is the distance be between two coordinate points, is given by

$$D_{ij} = \sqrt{(x_i(s)-x_j(s))^2 + (y_i(s)-y_j(s))^2} \quad i,j = 1,...,\mathrm{R}, i \neq j \tag{48}$$

where, 0< $S_{ij}$ <1. When $D_{ij}$ is small, $S_{ij}$ will be close to 1. Conversely, $S_{ij}$ will tend to zero if the $D_{ij}$ gets larger. In this way, $S_{ij}$ will have greater curvature, making it applicable to all data sets, not just the set of distances in a particular case. Mathematically, $\alpha$ is defined as

$$\alpha = -\ln 0.5 / \bar{D} \tag{49}$$

where, $\bar{D}$ is the mean distance among the pairs of coordinate points. When $S_{ij} > \beta$, the two coordinate points are considered largely relevant. $\beta$ is the threshold of similarity which takes a value in the range 0~1, and 0.7 is quite robust as shown by our experiments.

By traversing $R$ coordinate points, $R_i$ is regarded as the number point whose similarity with the *i-th* point is satisfied $S_{ij} > \beta$. Then the following hypothesis can be obtained.

$$\begin{cases} H_0 : R_i \geq R_s, & i = 1,...,R \\ H_1 : R_i < R_s, & i = 1,...,R \end{cases} \tag{50}$$

where, $R_s$ is the control coefficient of quantity with the range [0, R]. And it is better to take 20% of the total quantity. Then if $H_0$ is true, coordinate points are under LOS propagation. Or else coordinate points are outlier and removed.

*2) MFDAF for NLOS update:* MFDAF is used for data association and update in NLOS case, which based on fuzzy c-means clustering (FCM) and probabilistic data association (PDA). There are similar properties between the membership degree $u_{ij}$ of FCM and the association probability $\beta_{ij}$ of PDA. Therefore, the $\beta_{ij}$ can be replaced by $u_{ij}$ that has less complexity.

Firstly, supposed there is a set of data $Z_i$, and let $c$ and $C_j$ $(1 \leq j \leq c)$ respectively denote number of classes and center. The objective function based on FCM is modeled by

$$\begin{aligned} J(U,C) = K\sum_{i=1}^{n}\sum_{j=1}^{c} u^{\delta}_{ij}(Z_i - C_j)^T S_j^{-1}(Z_i - C_j) \\ + (1-K)\sum_{j=1}^{c}(C_j - F_j^p(Z_j)_{old})^T(C_j - F_j^p(Z_j)_{old}) \end{aligned} \tag{51}$$

subject to

$$\sum_{i=1}^{r} u_{ij} = 1, \quad 0 \leq u_{ij} \leq 1 \tag{52}$$

where, $\delta$ indicates the degree of ambiguity, which is used to modify the shape of membership functions under different categories. $(Z_j)_{old}$ is relevant knowledge of the last time of *j-th* class, which is a part of $\hat{X}(s-1|s-1)$, $F_j^p$ is the part of the matrix $F$ which represents the position component associated with the target $j$. Thus $F_j^p(Z_j)_{old}$ represents the predicted prototype of the j-th class. The last constant $K$ is a parameter ranging from 0 to 1, depending on whether we prefer the current observation or the known state. Generally, the value of $K$ should be greater than 0.5, which denotes that current observations are more trusted. Then $C_j$ and distance matrix $d_{ij}$ are be calculated as

$$\begin{aligned} C_j = \left[K\sum_{i=1}^{n} u^{\delta}_{ij} S_j^{-1} - (1-K)I\right]^{-1} \times \\ \left[K\sum_{i=1}^{n} u^{\delta}_{ij} S_j^{-1} Z_i - (1-K)F_j^p(Z_j)_{old}\right] \end{aligned} \tag{53}$$

$$d_{ij} = (Z_i - C_j)^T S_j^{-1}(Z_i - C_j) \tag{54}$$

the $u_{ij}$ can be updated to

$$u_{ij} = \frac{1}{\sum_{k=1}^{n}(d^2_{ij}/d^2_{kj})^{1/(\delta-1)}} \tag{55}$$

The objective function is minimized by iterating the $u_{ij}$ and $C_j$.

MFDAF has a significant effect in positioning of multi-target and single target. In this paper, we consider the case of one MN. Therefore, the $Z_i$ can be expressed as the coordinate estimation $Z_r(s)$ assumed by Eq. (50). Then the innovation $v_{2,r}(s)$ between prediction coordinate and $Z_r(s)$ is given by

$$v_{2,r}(s) = Z_r(s) - \hat{Z}(s|s-1) \tag{56}$$

where, $\hat{Z}(s|s-1)$ is the position estimation prediction, which given by

$$\hat{Z}(s|s-1) = G\hat{X}_2(s|s-1) \tag{57}$$

where, $G = \begin{bmatrix} 1 & 0 & 0 & 0 \\ 0 & 1 & 0 & 0 \end{bmatrix}$ is the observation matrix. Then let

$C_j = \hat{Z}(s \mid s-1)$ , $(Z_j)_{old} = \begin{bmatrix} X_{s|s-1}(1) \\ X_{s|s-1}(3) \end{bmatrix}$ and $F_j^p = \begin{bmatrix} 1 & 0 \\ 0 & 1 \end{bmatrix}$.

Finally, according to the probability calculated by Eq. (55), the state and variance vector can be updated. The innovation covariance matrix $S_2(s)$ and gain matrix $K_2(s)$ can be got by

$$S_2(s) = G\hat{P}_2(s \mid s-1)G^T + \sigma_i^2 I_2 \tag{58}$$

$$K_2(s) = \hat{P}_2(s \mid s-1)G^T S_2^{-1}(s) \tag{59}$$

Then the state and covariance are updated as

$$E(s) = \sum_{i=1}^{r} u_i(s) v_{r_i}(s) \tag{60}$$

$$\hat{X}_2(s \mid s) = \hat{X}_2(s \mid s-1) + K_2(s)E(s) \tag{61}$$

$$\hat{P}_2(s \mid s) = (I_4 - K_2(s)G)\hat{P}_2(s \mid s-1) + \tilde{P}_s \tag{62}$$

$$\tilde{P}_s = K(s)\left[\sum_{i=1}^{r} u_i(s) v^T{}_i(s) v_i(s) - E(s)E^T(s)\right] K_2{}^T(s) \tag{63}$$

$$\Lambda_2(s) = u_i(s) N(v_r(s); 0, S_2(s)) \tag{64}$$

where, $\tilde{P}_s$ with the weighted innovation $E(s)$ corrects the measurement uncertainty. And $\Lambda_2(s)$ indicates likelihood function.

### *E. IMM Model probability update and combination*

*1) Model probability update:* The probability of two models $\mu_j(s)$ can be updated

$$\mu_j(s) = (1/c)\Lambda_j(s)\overline{c}_j \tag{65}$$

where, $c$ denotes normalization factor, obtained by

$$c = \sum_j \Lambda_j(s)\overline{c}_j \tag{66}$$

*2) Combination:* The output state vector estimation $\hat{X}(s \mid s)$ and error covariance matrix $P(s \mid s)$ are

$$\hat{X}(s \mid s) = \sum_j \hat{X}_j(s \mid s)\mu_j(s) \tag{67}$$

$$\begin{aligned} P(s \mid s) = \sum_j \Big\{ & P_j(s \mid s) + \left[\hat{X}_j(s \mid s) - X(s \mid s)\right] \\ & \times \left[\hat{X}_j(s \mid s) - X(s \mid s)\right]^T \Big\} \mu_j(s \mid s) \end{aligned} \tag{68}$$

## IV. Simulation and Experimental Results

### *A. Simulation Results*

In this section, we designed simulations and experiments to verify the advantages of HT-MFDAF algorithm and it is compared with the existing localization algorithms. The MN is assumed to move along a fixed route in an area of $100m \times 100m$ that randomly distributed 6 BNs. The sample length is 100, and the sample interval is equal to 0.5. The initial state sector and covariance matrix of MN are $X(0) = [0m, 20m, 1m/s, 0.5m/s]^T$ and $P(0 \mid 0) = diag(1^2, 1^2, 1^2, 1^2)$ , the Markov transition matrix initial value was $p = \begin{bmatrix} 0.995 & 0.005 \\ 0.005 & 0.995 \end{bmatrix}$, and the error covariance is $R = I_N$, where $N$ denotes the number of base nodes.

Moreover the NLOS distance errors are randomly produced according to the probability $P_{NLOS}$ , which obeys Gaussian distribution. Particularly, in the NLOS recognition and verification phase, we let *L = 3*. The threshold $\lambda_{t1}$ , $\lambda_{t2}$ , $\lambda_{m1}$ and $\lambda_{m2}$ are calculated when the PFA is 80%, and can make $\sigma_{t1}$ and $\sigma_{t2}$ respectively equal to the STD of $S_1$ and $S_2$ in LOS propagation state. In order to get more accurate results, the simulation results are all obtained by 1000 Monte Carlo runs. We mainly compared PIMM (IMM-MPDA) [27], RIMM (IMM-REKF) [28] and EIMM (IMM-EKF) [29] with the same parameter.

Two indicators are used to evaluate the performance of the algorithm, which are cumulative distribution function (CDF) of the mean error distance (MED) and root mean square error (RMSE) respectively.

$$RMSE = \sqrt{\frac{1}{ST}\sum_{i=1}^{T}\sum_{s=1}^{S}((\hat{x}_i(s) - x(s))^2 + (\hat{y}_i(s) - y(s))^2)} \tag{69}$$

$$MED = \sqrt{\frac{1}{S}\sum_{s=1}^{S}((\hat{x}_i(s) - x(s))^2 + (\hat{y}_i(s) - y(s))^2)} \tag{70}$$

where, $S$ indicates the total number of time steps.

The NLOS error and measurement noise obey Gaussian distribution $N(0, \sigma_L{}^2)$ and $N(\mu_n, \sigma_n^2)$ respectively. The default parameters in this simulation are shown in Table I.

TABLE I.
THE DEFAULT PARAMETERS IN SIMULATION

| Parameter | Symbol | Default Values |
|---|---|---|
| Number of BN | N | 6 |
| Measurements noise | $N(0, \sigma_L{}^2)$ | $N(0, 1^2)$ |
| NLOS probability | $P_{NLOS}$ | 0.5 |
| NLOS error | $N(\mu_n, \sigma_n^2)$ | $N(5, 6^2)$ |

Fig. 10 - Fig. 12 illustrate that with the change of the $P_{NLOS}$ , $\mu_n$ and $\sigma_n^2$ , the RMSE comparison charts of four algorithms are displayed. It is worth noting that other parameters are the same.

It can be observed distinctly from Fig. 10, as the $P_{NLOS}$ increases, the positioning errors of all algorithms show an upward trend. This is because the error of measuring distance becomes larger due to the increase of $P_{NLOS}$ . When $P_{NLOS}$ is below 0.3, the performance of PIMM and HT-MFDAF is very close. However, as the $P_{NLOS}$ continues to rise, it is made evident that the precision of HT-MFDAF is superior to other algorithms, while the positioning error of PIMM increases at a faster speed. Based on the analysis above, it is not difficult to see that HT-MFDAF has strong robustness, especially in severe NLOS environments.

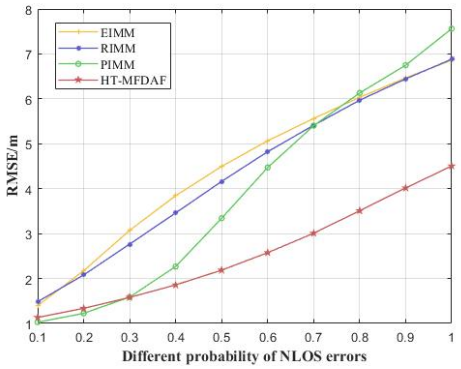


Fig. 10. Changes of RMSE under different $P_{NLOS}$ .

Fig. 11 distinctly reflects the change in RMSE when the $\mu_n$ increases from 2m to 9m. It is obvious that HT-MFDAF increases at a relatively slow speed and the accuracy is always higher than other algorithms, which is because HT-MFDAF takes $\mu_n$ into account when calculating thresholds. Meanwhile, the RMSE growth curve of other algorithms has a large slope In more details, the localization errors of PIMM, RIMM,EIMM and HT-MFDAF increase by 62.80% and 53.30%,54.50% and 23.09% respectively.

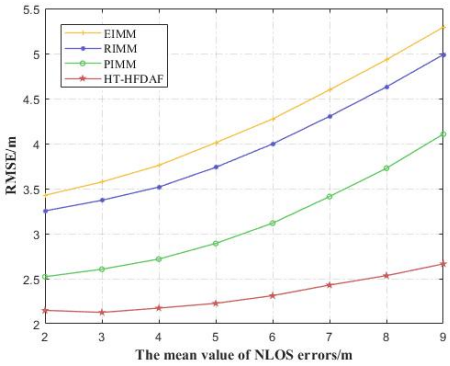


Fig. 11. Changes of RMSE under different $\mu_n$ .

It can be perceived that the Fig. 12 reveals to us the RMSE changes of $\sigma_n^2$ from 3 to 12.As the $\sigma_n^2$ increases, the positioning errors of EIMM and RIMM rises remarkably with the average accuracy 5.229m and 4.884m. By contrast, PIMM and HT-MFDAF rise relatively smoothly， because both algorithms recognize and process NOS according to $\sigma_n^2$ ,whose average location accuracy are respectively 3.492m and 2.426m.

Then CDF of MED is obtained by 1000 Monte Carlo simulations, which is shown in Fig. 13. The blue curve represents the CDF of the location error of HT-MFDAF, which has always been the fastest convergence. Furthermore, the 90% localization error of HT-MFDA, PIMM, RIMM and EIMM is less than 3.538 m, 5.468 m, 5.954 m and 6.008 m, respectively. From the data and figure, it is made evident that HT-MFDAF is significantly superior to other algorithms.

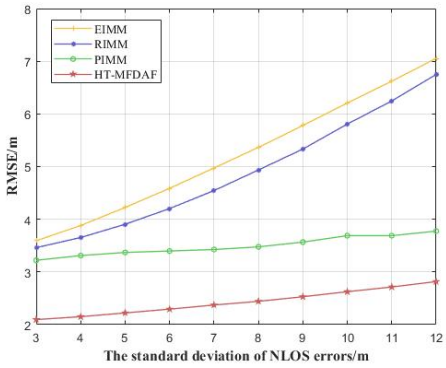


Fig. 12.Changes of RMSE under different $\sigma_n^2$ .

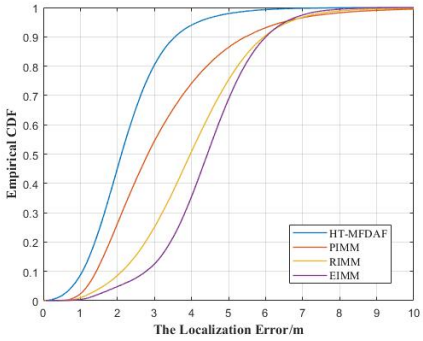


Fig. 13 CDF of positioning error.

## *B. Experimental Results*

To prove the effectiveness of HT-MFDAF, The experiment was set up in real indoor scenarios.

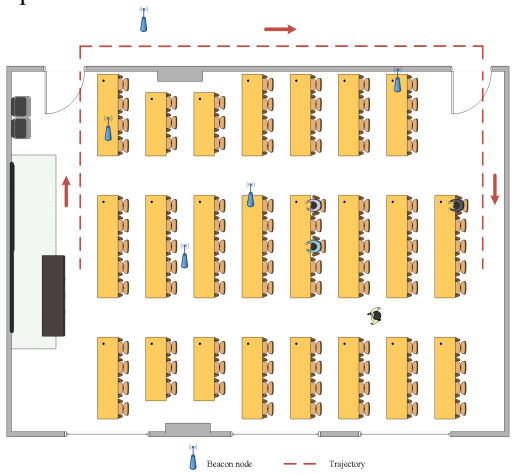


Fig. 14. Deployment of the environment.

The experiment is arranged in a $9.6m \times 8.4m$ classroom. The classroom, as shown in Fig. 14, is full of desks and chairs, which are students studying and moving around. 5 BNs have been set with position $BN_1(1.2m,1.8m)$ $BN_2(4.2m,0.6m)$ $BN_3(3.0m,3.0m)$ $BN_4(5.4m,6.6m)$ and $BN_5(7.2m,1.2m)$ . The red dotted line represents the moving track of MN, which follows the direction of the red arrow from classroom to hallway and last back to classroom. UWB is, in addition, used to obtain the distance between MN and BN, which has low transmission power and high positioning accuracy. We set up a total of 30 sampling points. It is worth noting that each

sampling point is, interval of 0.6 m, sampled 30 times, and taking the average as the last result.

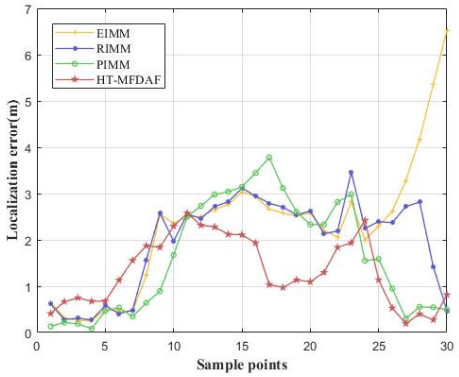


Fig. 15 Positioning error of each sampling point.

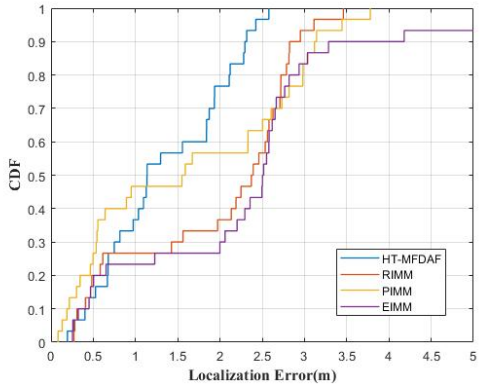


Fig. 16. CDF of positioning error.

To better evaluate the efficiency of HT-MFDAF, we conducted experiments under 4 BNs and 5 BNs respectively. It is worth to notice that the 4 BNs in the first experiment were all indoors. Therefore, when MN moves in the corridor, all the BNs are in the NLOS state. Fig demonstrates the positioning errors of the four algorithms, which can be observed that the positioning error of HT-MFDAF is less than EIMM, RIMM and PIMM at most sampling points, especially when all the BNs are in the case of NLOS propagation. Fig. 16 depicts the CDF of the positioning error. The 90% localization error of the HT-MFDAF is 2.316m. By comparison, the RIMM, PIMM and EIMM are achieved at 2.823m, 3.118m and 4.181m, respectively.

Next the BN in the corridor was added. Fig. 17 and Fig. 18 separately illustrate the positioning error of each sampling point and CDF of the positioning error. As can be observed from Figure 14, the positioning accuracy of HT-MFDAF is the highest at almost every sampling point. In more detail, the average positioning accuracy of HT-MFDAF is about 21.56%, 22.41% and 23.79% higher than that of the EIMM, RIMM and PIMM. From Fig. 18, HT-MFDAF still converges fastest. And the 90% localization error of HT-MFDA, EIMM, RIMM and PIMM is less than 2.699 m, 3.274m, 2.917m and 2.857 respectively. In summary, we verify that HT-MFDAF has better positioning performance through experiments.

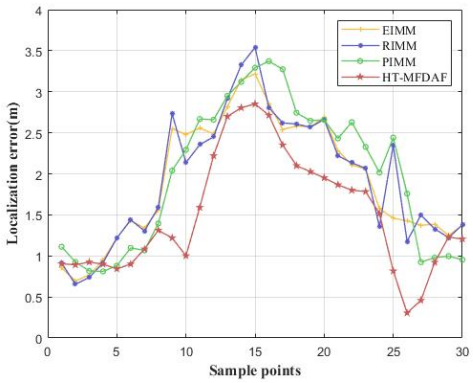


Fig. 17 Positioning error of each sampling point.

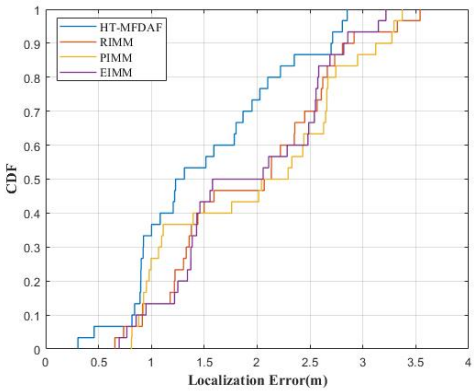


Fig. 18. CDF of positioning error.

## V. Conclusions And Future Works

A localization method based on hypothesis test for NLOS recognition and modified fuzzy probabilistic data association filtering (HT-MFDAF) is proposed in this paper. Firstly under the LOS model, EKF is used to update. Meanwhile, the initial distance measurements are processed by hypothesis test , under NLOS model, and then grouped and estimated by LS. A series of position estimates are obtained. Next the outliers are judged and abandoned by calculating the similarity. Finally the fuzzy membership degree of the remaining position estimation is calculated by MFDAF, reconstructing the correlation probability to get the position estimate. Simulations and experimental results, compared with PIMM, RIMM and EIMM, demonstrate the effectiveness of HT-MFDAF algorithm, especially in severe NLOS situations. When implementing the algorithm, prior knowledge of noise should be required for the hypothesis testing of the first stage. Or else, the information of noise has to compute in advance. Furthermore, HT-MFDAF can be more robustly applied to the tracking of different targets in more areas by building measurement models in the future work. And it can also be extended to the scene of multi-target tracking.

## Declarations section

### *A. Ethical Approval and Consent to participate*

Not applicable

### B. Human and Animal Ethics

Not applicable

### C. Consent for publication

All authors agree to publish in Peer-to-Peer Networking and Applications.

### D. Availability of supporting data

All data generated or analysed during this study are included in this article.

### E. Competing interests

The authors declare that there is no conflict of interests/competing interests regarding the publication of this paper.

### F. Funding

This work was supported by the National Natural Science Foundation of China under Grant No.61803077 and No. 61973069; Natural Science Foundation of Hebei Province under Grant No. F2020501012.

### G. Authors' contributions

Yan Wang and Yuxin Gong wrote the main manuscript text and Huikang Yang prepared figures 14-18. All authors reviewed the manuscript.

### H. Acknowledgements

Not applicable

### I. Authors' information

Yan Wang, Yuxin Gong, Huikang Yang are Department of Computer and Communication Engineering, Northeastern University, Qinhuangdao 066004, Hebei Province, China. (e-mail: wangyan_jgxy@neuq.edu.cn, 2172158@stu.neu.edu.cn , 2101922@stu.neu.edu.cn ).

## REFERENCES

[1] S. Verma, S. Zeadally, S. Kaur and A. K. Sharma, "Intelligent and Secure Clustering in Wireless Sensor Network (WSN)-Based Intelligent Transportation Systems," IEEE Transactions on Intelligent Transportation Systems, Nov. 2021.

[2] M. Anvaripour, M. Saif and M. Ahmadi, "A Novel Approach to Reliable Sensor Selection and Target Tracking in Sensor Networks," IEEE Transactions on Industrial Informatics, vol. 16, no. 1, pp. 171-182, Jan. 2020.

[3] P. Chanak and I. Banerjee, "Congestion Free Routing Mechanism for IoT-Enabled Wireless Sensor Networks for Smart Healthcare Applications," IEEE Transactions on Consumer Electronics, vol. 66, no. 3, pp. 223-232, Aug. 2020.

[4] A. Naeem, A. R. Javed, M. Rizwan, S. Abbas, J. C. -W.Lin, T. R. Gadekallu, "DARE-SEP: A Hybrid Approach of Distance Aware Residual Energy-Efficient SEP for WSN," IEEE Transactions on Green Communications and Networking, vol. 5, no. 2, pp. 611–621, June 2021.

[5] C. -H. Park and J. -H. Chang, "Robust Localization Based on ML-Type, Multi-Stage ML-Type, and Extrapolated Single Propagation UKF Methods Under Mixed LOS/NLOS Conditions," IEEE Transactions on Wireless Communications, vol. 19, no. 9, pp. 5819-5832, Sept. 2020.

[6] R. Liang et al., "Fault Location Method in Power Network by Applying Accurate Information of Arrival Time Differences of Modal Traveling Waves," IEEE Transactions on Industrial Informatics, vol. 16, no. 5, pp. 3124-3132, May. 2020.

[7] Chen L, Ahriz I, Ruyet D L, "AoA-Aware Probabilistic Indoor Location Fingerprinting Using Channel State Information," IEEE Internet of Things Journal, vol. 7, no. 11, pp. 10868-10883, Nov.2020.

[8] M. Zhou, Y. Li, M. J. Tahir, X. Geng, Y. Wang and W. He, "Integrated Statistical Test of Signal Distributions and Access Point Contributions for Wi-Fi Indoor Localization," IEEE Transactions on Vehicular Technology, vol. 70, no. 5, pp. 5057-5070, May 2021.

[9] Shixun Wu, Shengjun Zhang, Kai Xu, Darong Huang, "Probability Weighting Localization Algorithm Based on NLOS Identification in Wireless Network," Wireless Communications and Mobile Computing, 2019.

[10] N. Aghaie and M. A. Tinati, "Localization of WSN nodes based on NLOS identification using AOAs statistical information," 2016 24th Iranian Conference on Electrical Engineering (ICEE), pp. 496-501, 2016.

[11] Z. Deng, X. Zheng, C. Zhang, H. Wang, L. Yin and W. Liu, "A TDOA and PDR Fusion Method for 5G Indoor Localization Based on Virtual Base Stations in Unknown Areas," IEEE Access, vol. 8, pp. 225123-225133, 2020.

[12] W. Cui, B. Li, L. Zhang and W. Meng, "Robust Mobile Location Estimation in NLOS Environment Using GMM, IMM, and EKF," IEEE Systems Journal, vol. 13, no. 3, pp. 3490-3500, Sept. 2019.

[13] R. Sun, G. Wang, Z. Fan, T. Xu and W. Y. Ochieng, "An Integrated Urban Positioning Algorithm Using Matching, Particle Swam Optimized Adaptive Neuro Fuzzy Inference System and a Spatial City Model," IEEE Transactions on Vehicular Technology, vol. 69, no. 5, pp. 4842-4854, May 2020.

[14] L. Cheng, J. Hang, Y. Wang and Y. Bi, "A Fuzzy C-Means and Hierarchical Voting Based RSSI Quantify Localization Method for Wireless Sensor Network," IEEE Access, vol. 7, pp. 47411-47422, 2019.

[15] Y. Wang, K. Gu, Y. Wu, W. Dai and Y. Shen, "NLOS Effect Mitigation via Spatial Geometry Exploitation in Cooperative Localization," IEEE Transactions on Wireless Communications, vol. 19, no. 9, pp. 6037-6049, Sept. 2020.

[16] B. Silva and G. P. Hancke, "Ranging Error Mitigation for Through-the-Wall Non-Line-of-Sight Conditions," IEEE Transactions on Industrial Informatics, vol. 16, no. 11, pp. 6903-6911, Nov. 2020.

[17] J. Liao and B. Chen, "Robust Mobile Location Estimator with NLOS Mitigation using Interacting Multiple Model Algorithm," IEEE Transactions on Wireless Communications, vol. 5, no. 11, pp. 3002-3006, Nov. 2006.

[18] Zhang, Yi, Hong Song Chen, and Yuan Luo, "A Novel Infrared Landmark Indoor Positioning Method Based on Improved IMM-UKF," Mechanics and Materials, pp. 511–512 February 2014.

[19] Y. Sun, S. Yang, G. Wang and H. Chen, "Robust RSS-Based Source Localization With Unknown Model Parameters in Mixed LOS/NLOS Environments," IEEE Transactions on Vehicular Technology, vol. 70, no. 4, pp. 3926-3931, Apr. 2021.

[20] C. -H. Park and J. -H. Chang, "Robust Localization Based on ML-Type, Multi-Stage ML-Type, and Extrapolated Single Propagation UKF Methods Under Mixed LOS/NLOS Conditions," IEEE Transactions on Wireless Communications, vol. 19, no. 9, pp. 5819-5832, Sept. 2020.

[21] T. Ho, "Urban Location Estimation for Mobile Cellular Networks: A Fuzzy-Tuned Hybrid Systems Approach," IEEE Transactions on Wireless Communications, vol. 12, no. 5, pp. 2389-2399, May 2013.

[22] T. Ho, "Robust Urban Wireless Localization: Synergy Between Data Fusion, Modeling and Intelligent Estimation," IEEE Transactions on Wireless Communications, vol. 14, no. 2, pp. 685-697, Feb. 2015.

[23] C. Yang, B. Chen and F. Liao, "Mobile Location Estimation Using Fuzzy-Based IMM and Data Fusion," IEEE Transactions on Mobile Computing, vol. 9, no. 10, pp. 1424-1436, Oct. 2010.

[24] Mourad Oussalah, Joris De Schutter, "Hybrid fuzzy probabilistic data association filter and joint probabilistic data association filter," Information Sciences, vol.142, pp.195-226, May.2002.

[25] Li Liangqun, Ji Hongbing, Gao Xinbo, "Maximum entropy fuzzy clustering with application to real-time target tracking," Signal Processing, vol.86, pp3432-3447, Nov 2006.

[26] Gnane Swarnadh Satapathi, Pathipati Srihari, "Rough fuzzy joint probabilistic association for tracking multiple targets in the presence of ECM," Expert Systems with Applications, vol.106, pp.132-140, Sept.2018.

[27] Cheng, Xue, Liu, and Wang, "A Robust Tracking Algorithm Based on a Probability Data Association for a Wireless Sensor Network," Applied Sciences, vol. 10. Dec 2019.

[28] U. Hammes and A. M. Zoubir, "Robust MT Tracking Based on M-Estimation and Interacting Multiple Model Algorithm," IEEE

Transactions on Signal Processing, vol. 59, no. 7, pp. 3398-3409, July 2011.

[29] J. Liao and B. Chen, "Robust Mobile Location Estimator with NLOS Mitigation using Interacting Multiple Model Algorithm," IEEE Trans Wireless Communications, vol. 5, no. 11, pp. 3002-3006, Nov. 2006.